ENSO climate forcing of the marine mercury cycle in the Peruvian Upwelling Zone Does Not Affect Methylmercury Levels of Marine Avian Top Predators

Marina Renedo, David Point, Jeroen E. Sonke, Anne Lorrain, Hervé Demarcq, Michelle Graco, Daniel Grados, Dimitri Gutiérrez, Anaïs Médieu, Jean Marie Munaron, et al.

To cite this version:

Marina Renedo, David Point, Jeroen E. Sonke, Anne Lorrain, Hervé Demarcq, et al.. ENSO climate forcing of the marine mercury cycle in the Peruvian Upwelling Zone Does Not Affect Methylmercury Levels of Marine Avian Top Predators. Environmental Science and Technology, 2021, 55 (23), pp.15754-15765. 10.1021/acs.est.1c03861 . hal-03566681

HAL Id: hal-03566681
https://hal.umontpellier.fr/hal-03566681v1

Submitted on 20 Apr 2023

Environmental Science & Technology
2021, Volume 55, Issue 23, Pages 15754-15765
https://doi.org/10.1021/acs.est.1c03861
https://archimer.ifremer.fr/doc/00735/84742/

ENSO Climate Forcing of the Marine Mercury Cycle in the Peruvian Upwelling Zone Does Not Affect Methylmercury Levels of Marine Avian Top Predators

Renedo Marina [1, *] , Point David [1, *], Sonke Jeroen E. [1], Lorrain Anne [2], Demarcq Herve [3],
Graco Michelle [4], Grados Daniel [4], Gutiérrez Dimitri [4], Médieu Anais [2], Munaron Jean-Marie [2],
Pietri Alice [4], Colas François [5], Tremblay Yann [3], Roy Amedee [3], Bertrand Arnaud [3],
Lanco Bertrand Sophie [3]

[1] Géosciences Environnement Toulouse (GET)-Institut de Recherche pour le Développement (IRD), CNRS, Université de Toulouse, 14 Avenue Edouard Belin, Toulouse 31400, France
[2] Univ Brest, CNRS, IRD, Ifremer, LEMAR, Plouzané F-29280, France
[3] IRD, MARBEC (Univ. Montpellier, CNRS, Ifremer, IRD), Sète 34203, France
[4] Instituto del Mar del Perú (IMARPE), LOCEAN IPSL (IRD/CNRS/SU/MNHN)Esquina Gamarra y General Valle, Callao 07021, Peru
[5] LOCEAN IPSL (IRD/CNRS/SU/MNHN), 4 Place Jussieu, Paris 75252, France

* Corresponding authors : Marina Renedo, email address : mrenedoelizalde@gmail.com ; David Point, email address : david.point@ird.fr

Abstract :

Climate change is expected to affect marine mercury (Hg) biogeochemistry and biomagnification. Recent modeling work suggested that ocean warming increases methylmercury (MeHg) levels in fish. Here, we studied the influence of El Niño Southern Oscillations (ENSO) on Hg concentrations and stable isotopes in time series of seabird blood from the Peruvian upwelling and oxygen minimum zone. Between 2009 and 2016, La Niña (2011) and El Niño conditions (2015–2016) were accompanied by sea surface temperature anomalies up to 3 °C, oxycline depth change (20–100 m), and strong primary production gradients. Seabird Hg levels were stable and did not co-vary significantly with oceanographic parameters, nor with anchovy biomass, the primary dietary source to seabirds (90%). In contrast, seabird Δ199Hg, proxy for marine photochemical MeHg breakdown, and δ15N showed strong interannual variability (up to 0.8 and 3‰, respectively) and sharply decreased during El Niño. We suggest that lower Δ199Hg during El Niño represents reduced MeHg photodegradation due to the deepening of the oxycline. This process was balanced by equally reduced Hg methylation due to reduced productivity, carbon export, and remineralization. The non-dependence of seabird MeHg levels on strong ENSO variability suggests that marine predator MeHg levels may not be as sensitive to climate change as is currently thought.

Graphical abstract

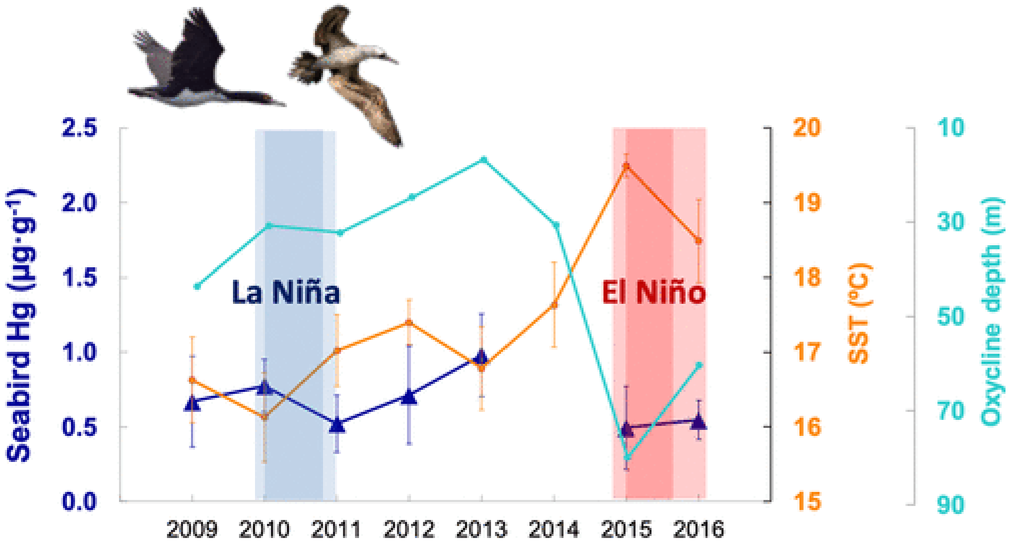

Keywords : Hg stable isotopes, MIF, Northern Humboldt current system, climate change, ecology

1 Introduction

Mercury (Hg) is a pollutant of major concern, efficiently bioassimilated and bioaccumulated in its methylmercury form (MeHg). It poses risks for the health of marine top predators, and humans who are mainly exposed to MeHg via seafood consumption [1]. In the industrial era, anthropogenic Hg emissions have exceeded natural volcanic and soil degassing emissions by a factor of seven [2], resulting in similar enrichment of atmospheric and surface ocean Hg levels [2,3]. The biogeochemical Hg cycle is highly complex and comprises multiple chemical and biological transformations that control marine MeHg formation, breakdown and bioavailability to marine organisms, such as methylation/demethylation, redox reactions or photochemical processes. Mercury methylation is thought to be mainly driven by anaerobic micro-organisms within the water column, with a peak in net MeHg production at depth, in oceanic oxygen minimum zones (OMZ) [4–6] where organic matter remineralisation rates are the highest. Consequently, the depth of occurrence of pelagic fish has been identified as a prominent control factor on MeHg concentrations in marine predators [7].

The impact of climate change forcing on the net production of marine MeHg represents a yet unknown and critical focal point of Hg research [8–10]. Global estimations predict rising seawater temperatures of 1.1 to 2ºC by 2100 depending on emission scenarios [11], an enhanced level of ocean acidification and oxygen loss [12], reduced ocean primary production [13] and the expansion of OMZ [14,15]. Global warming is also expected to cause the loss of coastal resources and reduce the productivity of fisheries and aquaculture, with fisheries models estimating a decrease of 1.5 to 3.4 million tons of annual global marine fisheries catches during the 21st century [16,17]. These changes in oceanographic dynamics, primary production, OMZ extension and ocean-atmosphere exchanges can potentially influence marine MeHg production, bioavailability and transfer in the food web [8,10,18]. Experimental studies on estuarine and freshwater fish showed that rising water temperatures could increase MeHg bioaccumulation levels [19,20]. A recent modelling study also predicted increasing trends of MeHg concentrations in fish from the Gulf of Maine due to warmer seawater temperatures [9]. The authors also suggested that overfishing could lead to enhanced MeHg accumulation in some marine fish species due to subsequent dietary shifts [9]. However, modelling studies present limitations relative to the most probable warming scenarios, and the complex connections between biogeochemical and ecological processes operating at regional and global scales. Experimental studies and long-term observations in relevant warming marine ecosystems are needed to help capture the complexity and coupling between baseline and trophic processes that govern MeHg concentrations in the food web.

The Northern Humboldt Current System (NHCS) off Peru [21,22] represents a unique ecosystem to explore the influence of ocean warming on marine biogeochemistry and ecology in the context of the climate forcing induced by El Niño Southern Oscillations (ENSO) [22]. The NHCS is one of the most productive regions of the global ocean [23], exhibiting the most extensive and shallow OMZ [22,24] on earth, and accounting for >10% of global fisheries, and particularly anchovy (*Engraulis ringens*) [23]. The shallow oxycline (∼20–100 m) acts as a physical barrier for fish biomass, which is mostly concentrated at the surface. The oxycline is also the relevant interface for the formation of MeHg. A high proportion of dissolved MeHg (relative to total Hg) has been documented in this region in surface waters compared to other parts of the Pacific Ocean [25,26]. Every 2–7 years, ENSO events strongly affect marine primary productivity and food web dynamics. During extreme Eastern Pacific (EP) El Niño events, the reduced wind speed along the Peruvian coast leads to a decreased upwelling circulation that brings normally deep cold nutrient rich waters to the surface sustaining the high productivity of this region [21]. Under El Niño conditions, the thermocline, nitracline and oxycline deepen significantly and the water column becomes more oxygenated at the surface, leading to warmer surface temperature anomalies [24]. Under these circumstances, the food web is particularly affected since the phytoplankton growth is strongly reduced. This impacts the whole ecosystem leading to a reduced fish biomass potentially influencing the food web structure , causing a high mortality of marine top predators [27], but also impacting fishery catch [28,29].

In this work, we investigated how climate forcing induced by ENSO in the NHCS, influences MeHg biogeochemistry and concentrations at the top of the marine food web. We hypothesized that the warming conditions and the deepening of the oxycline during El Niño events would change the depth at which MeHg is produced, likely decreasing its photodegradation, possibly favouring its production, bioavailability and concentration further in the food chain. We also explored and discussed how complementary and compensating processes could mitigate the production of MeHg and its concentration in the food chain during these events due to the reduced vertical export of organic matter toward the oxycline. Our strategy consisted of documenting and discussing the role of ENSO through the change of the environmental, physical and oceanic biogeochemical variables on Hg concentrations and Hg stable isotopic composition in a 8 year time series of blood samples from two key sentinel avian top predators : the Peruvian booby *Sula variegata* and the Guanay cormorant *Phalacrocorax bougainvillii*, that are known to feed almost exclusively (90% on average) on anchovy [30,31]. Mercury concentration in seabird blood has been documented to be a very sensitive proxy of MeHg levels and bioavailability in the local and regional marine ecosystem [32,33]. Blood Hg isotopic composition of seabirds efficiently reflects recent Hg exposure [34] (i.e. 2-5 weeks preceding sampling [35]), and can provide major clues to elucidate the marine Hg cycle [36,37]. Mercury stable isotopes has greatly improved knowledge on the sources of exposure, transfer pathways, and metabolism of Hg in marine consumers [36,38,39]. Many abiotic (e.g. photoreduction, volatilization) [40,41] and biotic processes (e.g. methylation, demethylation) [42–44] result in mass-dependent isotope fractionation (MDF, reported as δ^{202}Hg). By contrast, mass-independent fractionation of odd-mass number isotopes (odd-MIF, reported as Δ^{199}Hg or

Δ^{201}Hg) has been primarily observed during aquatic photochemical reactions [40], and is preserved during biological or trophic processes [45]. The systematic decline in Δ^{199}Hg observed in marine organisms with the depth at which they feed has been attributed to the decrease of MeHg photodegradation in the water column, allowing to demonstrate that MeHg is mainly produced in the OMZ [38]. This proxy is thus particularly relevant in the context of the present study. Carbon (δ^{13}C) and nitrogen (δ^{15}N) stable isotopes were also determined to provide insights about the foraging ecology of the seabird species, and to detail the influence of isotopic baseline variations during contrasted upwelling regimes [46–49] on Hg concentrations and stable isotopes.

2 Materials and methods

2.1 Sample collection

Sampling was conducted from 2009 to 2016 (except 2014) during the months of October-November at Pescadores Island, Peru (11°46′S, 77°15′W) which correspond to the breeding period. During that time, seabirds are restricted to their nesting area making Hg concentrations and stable isotope data only representative of their breeding grounds in the NHCS. Individuals of Guanay cormorants and Peruvian boobies were randomly chosen during each sampling campaign. Each bird was measured, weighed and sexed as detailed in a previous work [31]. Birds were breeders (breeding 1-4 weeks old chicks at the time of sampling) or juveniles. Some individuals of boobies and cormorants were equipped with GPS recorders for spatial tracking of their foraging trips and time-depth recorders to track their diving behaviour [31]. The two seabird species slightly differ on their foraging strategies in terms of diving depths, with cormorants presenting better diving capacities than boobies [31]. No sex-related differences in foraging habits have been observed between males and females of the two species [31]. Blood samples were collected from a wing or tarsal vein and preserved in 70% ethanol [49]. Samples of ingested anchovies (standard length of 12-13 cm) were also collected and preserved similarly in 70% ethanol when the birds regurgitated spontaneously. No other prey was observed. Prior analysis, blood and prey samples were dried, lyophilized and grounded. The number of seabird individuals and prey analysed for Hg concentrations, C, N isotope analysis ranged from 5 to 41 individuals per species depending on the year, while Hg isotope analysis was performed in 4 to 10 chosen individuals, per species per year, based on the sample mass available.

2.2 Analytical methods

Total Hg concentrations

Total Hg concentrations, hereafter expressed in $\mu g\ g^{-1}$ of dry weight (dw), were quantified by using a DMA80 analyzer (Milestone, USA). The detection limit was 0.005 $\mu g \cdot g^{-1}$ dw. Three certified reference materials were analysed for evaluation of accuracy and reproducibility of our methods: tuna fish muscle (ERM-CE-464 and IAEA-436) and lobster hepatopancreas material (TORT-3); providing a respective accuracy of 96±12% (n=15), 96±9% (n=6), and 100±9% (n=6) relative to recommended reference values. Internal homemade blood reference material (red blood cells, RBC-KP) was also used for validation of seabird blood analyses and provided an accuracy of 96±6% (n=3) relative to previously published values, as detailed elsewhere [34].

Total Hg isotopic analyses

Blood samples (0.05–0.10 g) were soaked in 3 or 5 mL of concentrated bi-distilled HNO_3 (~11N) overnight at room temperature then heated on a hotplate at 80 °C during 6 h (4 h in HNO_3 and 2 h more after addition of 1/3 of the total volume of H_2O_2 30%, ULTREX quality). We added 100 µL of BrCl (0.2 mol L^{-1}) to convert all MeHg to inorganic Hg. The digest mixtures were finally diluted in inverse aqua regia (3 HNO_3: 1 HCl). Final Hg concentrations ranged from 0.5 to 1 $ng \cdot g^{-1}$.

Mercury isotopic composition was measured using a multicollector inductively coupled to plasma mass spectrometry (MC−ICP−MS, Thermo Finnigan Neptune Plus) with continuous-flow cold vapor (CV) generation using Sn (II) reduction (CETAC HGX-200). Mercury isotopic values were reported as delta notation, calculated relative to the bracketing standard NIST SRM-3133 reference material to allow interlaboratory comparisons, as described in the SI. Secondary standard NIST RM-8160 (previously UM-Almadén standard) was used for validation of the analytical session (Table S1). Recoveries of extraction (102±17%, mean±SD) were calculated for all samples (n=87) by checking the signal intensity obtained on the MC-ICPMS for diluted extracts relative to NIST 3133 standard (with an approximate uncertainty of ±15%). Certified reference materials (ERM-CE-464 and IAEA-436) and the internal blood reference material (RBC-KP) were also measured (Table S1). Uncertainty for delta values was based on 2SD errors for each certified reference material (Table S1).

Carbon and nitrogen stable isotopic analyses

Blood samples were freeze-dried and powdered, and subsamples were weighed with a microbalance and packed in tin containers. Carbon and nitrogen stable isotope ratios were determined in total seabird blood and anchovies with a continuous flow mass spectrometer (Delta V Advantage with a Conflo IV interface, Thermo Scientific, Bremen, Germany) coupled to an elemental analyser (Flash EA1112, Thermo Scientific, Milan, Italy). Results are in delta notation relative to Vienna PeeDee Belemnite and atmospheric N_2 for $\delta^{13}C$ and $\delta^{15}N$, respectively. Replicate measurements of internal laboratory standards (acetanilide) indicated measurement errors <0.15‰ for both $\delta^{13}C$ and $\delta^{15}N$ values.

2.3 Environmental parameters

The spatio-temporal variability of the main marine physical and biogeochemical parameters of seabird foraging areas was derived from satellite and acoustic observations. Satellite datasets of sea-surface temperature (SST), net primary productivity (NPP), wind speed, diffuse attenuation coefficient Kd490, photosynthetically available radiation (PAR), total kinetic energy (TKE) and upwelling index (Ekman transport), were integrated at three different spatial scales, respectively from the coast to 80, 100 and 150 km offshore: small-scale A1 (lat: 12.5-11.0°S); medium-scale A2 (lat: 13.5-10.5°S) and large-scale A3 (lat: 14.0-9.5°S). The small-scale spatial integration (A1) is based on the tracking data of the main seabird trajectories [31] and reflects their effective foraging zone (Figure 1). We know that seabirds are restricted to foraging areas near their colonies during their breeding period due to the need to frequently feed their chicks. However, since MeHg accumulated in seabirds is mainly transferred from anchovies that integrate larger areas [50,51], we also treated the environmental data at large scale area (A3) based on anchovy biomass distribution [50,52] for the considered period. Medium-scale area A2 was also considered as an intermediate area between A1 and A3 (Figure S1).

Seabird blood represents exposure over the last 2 to 5 weeks preceding sampling [34], i.e. October-November. We therefore calculated mean values (and standard error, SE) of each environmental parameter for the period from the 1st October to 30th November. All environmental satellite variables were averaged at monthly resolution. Anomalies of the environmental variables were calculated relative to mean seasonal values for the 2009-2016 period.

Oxycline depth variations were recorded by acoustic measurements based on the depth of the vertical extension of the epipelagic community as explained in previous work and specific for this area [53]. Acoustic oxycline data were previously compared and validated with *in situ* dissolved oxygen concentration analyses from the period October-December in Callao station (estimation of oxycline at DO=22 μmol Kg^{-1}, see [22,54] for more details). Acoustic data used in this work were processed at the three integrated areas A1, A2 and A3 with respective spatial resolutions (0.5, 1 and 2 degrees and 50 meters of acoustic data resolution) and integrated during the period of October to November. Acoustic data of 2013 were only available for the period February-April, so we estimated the oxycline depth values for October-November 2013 by extrapolation validated with the correlation between oxycline depth and SST anomalies for the three spatial areas.

Anchovy total biomass (mean ± SE) was determined by acoustic observations and integrated for a large spatial coastal area (8 to 16°S) corresponding to the spring survey (October-November) using the methodology developed by Simmonds and co-workers [55]. Data of anchovy fish captures were provided by the FAO (Food and Agriculture Organization of the United Nations [56]) for the Major Fishing Area in the southeast Pacific Ocean and by the Ministry of Production of Peru [57]. The variability of ENSO was determined by the ICEN (Coastal El Niño Index), which is a regional (Eastern Pacific) index of ENSO activity in the region of Peru provided by the Technical Committee of the National Study of the El Niño Phenomenon (ENFEN) [58]

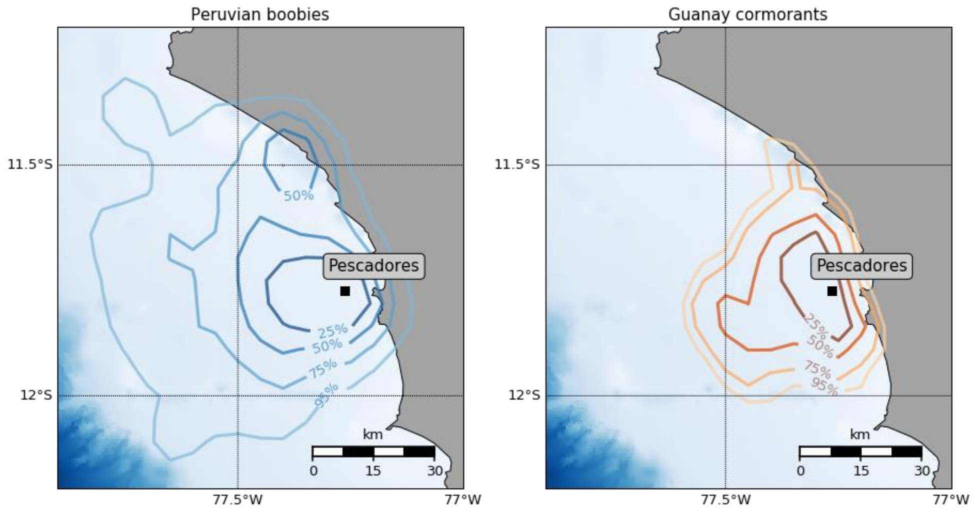

Figure 1. Seabird foraging area over the 2009-2015 period: kernel of dive density estimations for boobies (left panel) and cormorants (right panel).

2.4 Statistical tests

Statistical analyses were performed using the software R 3.3.2 [59]. Data were first checked for normality of distribution and homogeneity of variances using Shapiro–Wilk and Breusch-Pagan tests, respectively. Statistical significance of the temporal variations of Hg concentrations, C, N and Hg isotopic composition were examined using a linear regression fitted along years. Statistical differences between years were investigated by non-parametrical tests (Kruskal–Wallis with Conover-Iman post-hoc test) since data did not meet specificities of normality and homoscedasticity. Interspecies differences were also tested statistically by Wilcoxon tests. Statistical significance was set at $p<0.05$.

We used generalized additive models (GAM) [60] to assess the influence of environmental parameters in explaining the interannual variations of seabird Hg concentrations and isotopic signatures of the NHCS. GAM tests were fitted in R using the mgcv package [61]. Response variables (blood Hg concentrations converted into log(Hg), δ^{202}Hg and Δ^{199}Hg values were assumed to follow a Gaussian distribution. Explanatory variables tested included ecological factors (δ^{15}N and δ^{13}C values) and oceanographic parameters (oxycline depth, SST, ICEN index, chlorophyll-a concentration, NPP, wind speed, diffuse attenuation coefficient Kd490, PAR, coastal upwelling index, TKE and anchovy biomass). Multi-colinearity was checked by calculation of the variance inflation factor (VIF) [62]. Only the parameters whose VIF<2 were considered in the GAM models. ICEN index was found to be collinear to other variables and was removed from the explanatory variables. Chlorophyll-a concentrations, PAR and NPP were highly correlated, so we only tested these variables separately in the GAM models. All the explanatory variables were fitted in the GAM with a low spline complexity ($k = 3$) to reduce over-fitting. The best-fit GAM models were selected by using the Akaike's Information Criterion (AICc) corrected for small samples sizes [60]. Additionally, we examined the fitted GAM models with diagnostic plots of residuals. To determine the amount of variation explained by each explanatory variable, we fitted a separate model for individual variable. The deviance explained (% DE) for each model was compared to assess the capacity of prediction of each model. Results of GAM tests are included in the SI (Table S2).

3 Results & discussion

3.1 Humboldt ENSO events: physical and biogeochemical dynamics

Monthly-averaged ICEN index shows the ENSO variability for the period 2009-2016 (Figure 2A). The intensity of the events (weak, moderate, strong) was also based on the ICEN index diagnostic of the ENFEN [58,63]. The impact of a given ENSO event on the Peruvian upwelling system depends on its magnitude and the spatial structure. El Niño events that develop in the Central-Pacific (called CP El Niño or Modoki) do not induce significant warming of the surface waters off the shelf of Peru, contrary to extreme and Eastern Pacific El Niño events (EP El Niño) [64,65]. The definition used for the ENFEN to classify extreme ENSO events requires the registration during more than three consecutive months of an ICEN index > 1 ºC for El Niño and < -1.2 ºC for La Niña events [58,63]. The period of 2009-2010 was classified as a weak CP El Niño (ICEN index of 0.7 ºC) exhibiting a very limited influence on the Peruvian coast [29], so was not considered in this study. However, an extreme EP El Niño occurred during the 2015-2016 period (ICEN index of 2.2 ºC) affecting the NHCS. The period from mid-2010 to early 2011 was classified as a moderate La Niña event (ICEN index of −1.3 °C).

Despite a medium but sustained yearly upwelling intensity during the study period, a relatively high persistent upwelling index was observed in late 2015 (Figure 2B). Positive SST anomalies (≈+2ºC) were observed both in 2015 and 2016, which corresponds to the signature of extreme EP El Niño conditions (Figure 2C). The warming of surface waters during El Niño is caused by downwelling equatorial Kelvin waves generated by wind anomalies in the western equatorial Pacific [66]. During El Niño events, the relatively warmer and deeper mixed layer decreases water ventilation and upwelling of deep cold-water masses is reduced which translates into a significant deepening of the oxycline in our study area (from 40 to ~90 m depth) in 2015 (Figure 2D), whereas in normal conditions the oxycline depth (OMZ=22 µmol Kg^{-1}) oscillates between 15 to 25 m depth [24]. This strong vertical deepening of the oxycline is in agreement with previous observations [54,67] and consistent with El Niño peak phase (November-December 2015).

The NPP off the Peruvian upwelling system was relatively stable during the period 2009-2016 and varied within the typically observed ranges for this ecosystem (1.8 to 5.2 g C m^{-2} day^{-1}, [68]) (Figure 2E). El Niño 2015-2016 did not strongly impact primary production in the eastern Pacific, compared to past extreme EP El Niño events [69]. During La Niña 2010-2011, the average NPP during the spring period exhibited a maximum, particularly in the spatial area near the coast A1 (4.8 gC m^{-2} day^{-1}). This year also accounted for an exceptionally large anchovy biomass (~7 million tonnes). On average, enhanced global biomass of approximately +1.1 million tonnes are observed during strong La Niña years [29]. In contrast, EP and extreme El Niño events commonly result in reduced global landings, with anomalies of −0.7 to −3.2 million tonnes depending on the intensity of the event (Figure 2F) [29]. Therefore, strong El Niño conditions in 2015-2016 and La Niña event occurring in 2010-2011 resulted in strong variability of climatic conditions of the Peruvian ecosystem, with SST anomalies of ±3°C, oxycline variability from 20 to 100 m depth and large range of NPP and biomass gradients.

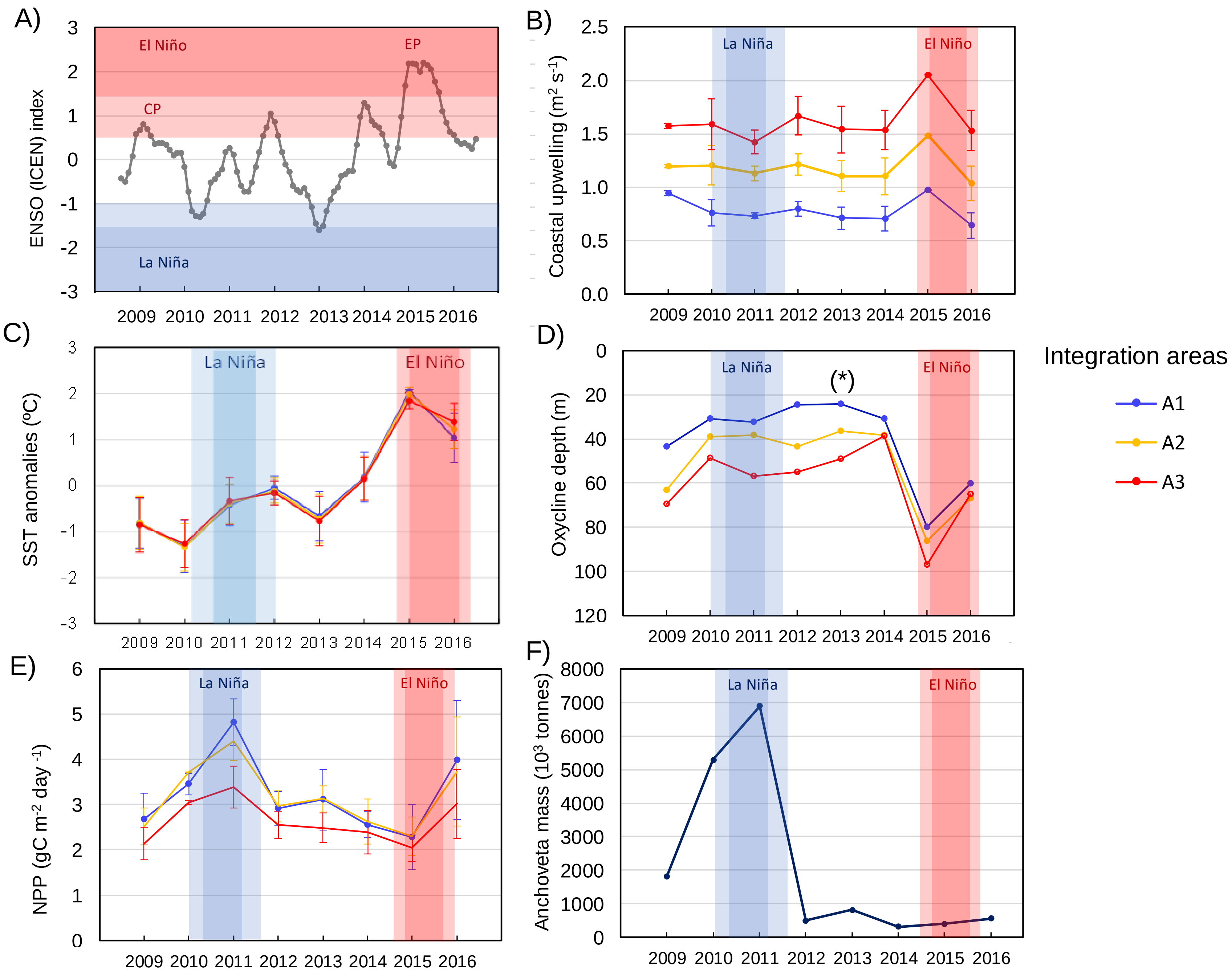
A)
ENSO (ICEN) index
El Niño
EP
CP
La Niña
3
2
1
0
-1
-2
-3
2009 2010 2011 2012 2013 2014 2015 2016
B)
Coastal upwelling ($m^2 s^{-1}$)
La Niña
El Niño
2.5
2.0
1.5
1.0
0.5
0.0
2009 2010 2011 2012 2013 2014 2015 2016
C)
SST anomalies (ºC)
La Niña
El Niño
3
2
1
0
-1
-2
-3
2009 2010 2011 2012 2013 2014 2015 2016
D)
Oxycline depth (m)
La Niña
El Niño
(*)
0
20
40
60
80
100
120
2009 2010 2011 2012 2013 2014 2015 2016
Integration areas
A1
A2
A3
E)
NPP (gC m^{-2} day^{-1})
La Niña
El Niño
6
5
4
3
2
1
0
2009 2010 2011 2012 2013 2014 2015 2016
F)
Anchoveta mass (10^3 tonnes)
La Niña
El Niño
8000
7000
6000
5000
4000
3000
2000
1000
0
2009 2010 2011 2012 2013 2014 2015 2016

Figure 2. Interannual variations of 2-month means (1st October to 30th November) of physical and biogeochemical/biological parameters measured in the Humboldt upwelling region. A) ENSO index (as regional Coastal El Niño index, ICEN): El Niño event in red (CP and EP refer respectively to Central Pacific and Eastern Pacific El Niño events) and La Niña event in blue, B) Coastal upwelling index (m^2 s^{-1}, Ekman transport), C) Sea surface temperature anomalies (°C), D) Oxycline depth (m), E) Net primary production (mg $C.m^{-2}.day^{-1}$), F) Anchoveta total biomass (in 10^3 tons). Values are means ± standard error for the total number of observations over the 2-month period. (*) Values of oxycline depth for 2013 for the period October-November are estimated by extrapolation from the correlation of recorded SST anomalies and oxycline depth data available for the period February-April 2013.

3.2 Relation of seabird isotopes to their specific foraging habits.

Similar to previous works, we assumed here that total Hg concentration and Hg isotopic composition in seabird blood represent the dominant (>90%) MeHg fraction [36,37]. Overall blood Hg concentrations (mean ± SD; min-max) were consistently higher in Guanay cormorants (0.86 ± 0.34; 0.23-1.81 µg $\cdot g^{-1}$, n=118) than in Peruvian boobies (0.57 ± 0.21; 0.13-1.29 µg $\cdot g^{-1}$, n=110) for the period considered (Wilcoxon test, $p<0.001$). Fieldwork revealed almost no other preys than anchovy in seabird regurgitate, confirming that both Guanay cormorants and Peruvian boobies mainly prey upon anchovies with a similar relative importance of 81–96% and 80–93% of their diets, respectively [30,70]. The offset of blood Hg levels between the two species may be due to slight differences in their foraging habits and/or or species-specific metabolic response to Hg [36,71].

A decreasing trend of $\delta^{13}C$ values from coastal to oceanic zones is commonly observed in many marine ecosystems, including the Peruvian upwelling system [46], because $\delta^{13}C$ values of particulate organic matter decrease from inshore to offshore waters due to the reduction of productivity [68,72]. Consistently lower $\delta^{13}C$ values of Guanay cormorants relative to Peruvian boobies ($p<0.001$) over the studied period (Figure S4) are therefore consistent with cormorants using more inshore foraging habitats, as shown in Figure 1. Guanay cormorants are known to have excellent diving capacities up to 32 m depth [31], then covering potentially the deep vertical range of the anchovy aggregations, while Peruvian boobies target the extended horizontal range of anchovy schools [31,73]. Similarly, $\delta^{13}C$ values of particulate organic matter are related to water depth [74] so the vertical foraging habitats of seabirds could also influence their C isotopic values, in line with the distribution of anchovy schools distributed above the oxycline [75].

Guanay cormorants presented only slightly higher $\delta^{15}N$ values (0.2 to 0.5‰ of mean difference) than Peruvian boobies (Wilcoxon test, $p<0.001$), except in 2016. This suggests that the two seabird species forage at a near similar trophic level and on very close prey items. The limited but significant differences in both $\delta^{13}C$ and $\delta^{15}N$ among the two-seabird species could reflect slight variations of their foraging habits and specialisation in line with the variability of the aggregation and distribution of anchovy schools between the surface and the oxycline. Differences in seabird metabolism could also explain the slight differences observed, as for Hg. However, these results confirm that both seabird species forage essentially on anchovy schools (Figure S4) confirming the field work observations by our team[30,70]. As detailed in section 3.4, we found that during el Niño events, a reduced denitrification associated with a deeper oxycline [76] is mostly responsible for the interannual differences in $\delta^{15}N$ in seabirds, and for the rest of the food web [48].

Individual bird blood $\delta^{202}Hg$ (MDF) showed moderate variability both for Guanay cormorants (0.41-1.49‰) and Peruvian boobies (0.28-1.37‰). Overall, the two species presented statistically different $\delta^{202}Hg$ values (Kruskal Wallis, $H=8.144$, $p=0.004$), especially during 2009 and 2010 in which cormorants displayed 0.5‰ higher mean values than boobies (Figure 3). Significant correlation between Hg concentration and $\delta^{202}Hg$ values was observed in seabirds ($R^2=0.51$, $p<0.0001$, $n=72$, Figure S7) although it was not significant for anchovies ($p=0.06$, $n=14$). Mass dependent fractionation of Hg isotopes occurs during many physical, chemical or biological processes [41,77–79]. The influence of biological and ecological factors on $\delta^{202}Hg$ values shows the limitation of this type of signature to trace which Hg transformations occur during ENSO-related variations. The interpretation of seabird $\delta^{202}Hg$ values as a proxy of changing environmental conditions requires a complete knowledge of all the processes and factors driving Hg MDF, especially when using biological models such as seabirds (i.e., trophic ecology and intrinsic metabolic/physiological processes). For instance, seabird δ^{202}Hg values are known to be sensitive to their specific foraging habitats [36]. Higher Hg concentrations and δ^{202}Hg values of Guanay cormorants support that this species targets larger size and deeper anchovy aggregations than Peruvian boobies. Both seabird species exhibited significantly higher δ^{202}Hg values than anchovy (mean difference of 0.9‰). This is in good agreement with the Hg MDF commonly observed in predator-prey and is thought to reflect the partial metabolic breakdown of MeHg, which leads to bioaccumulation of isotopically heavier MeHg in birds, sharks and mammals [42,80,81]. The lower blood Hg levels in Peruvian boobies are accompanied by lower δ^{202}Hg (i.e. less demethylated MeHg), suggesting that species-specific metabolic MeHg breakdown is not a major control factor on blood Hg.

We observed similar variability of Δ^{199}Hg (Hg odd-MIF) between Guanay cormorants (1.63-2.60‰) and Peruvian boobies (1.70-2.57‰) (Kruskal Wallis, H=2.117, p=0.146). Positive Δ^{199}Hg in aquatic food webs are mainly due to the photochemical processes prior to MeHg incorporation into food webs, then preserving the Δ^{199}Hg baseline signature [40]. This is confirmed by the Δ^{199}Hg/Δ^{201}Hg of 1.15±0.09 (SE) of anchovy and 1.02±0.05 (SE) of seabirds (Figure S5). Overall Δ^{199}Hg values of anchovies (2.04±0.37‰, n=14) were similar to Δ^{199}Hg values of seabirds (2.08±0.24‰, n=72) (H=4.89, p=0.09), which is coherent with the absence of Hg odd-MIF during trophic transfer [45], and confirms that the seabirds feed predominantly on anchovy. A consistent decrease of fish Δ^{199}Hg with the foraging depth has been observed in the open Pacific ocean due to the dilution of surface photodegraded MeHg by in situ methylated Hg at depth [38]. Although the two seabird species slightly differ in their foraging depth [31], their similar Δ^{199}Hg values suggest that both accumulate MeHg that has undergone similar degrees of photodemethylation in the water column confirming that both species rely on similar anchovy aggregations.

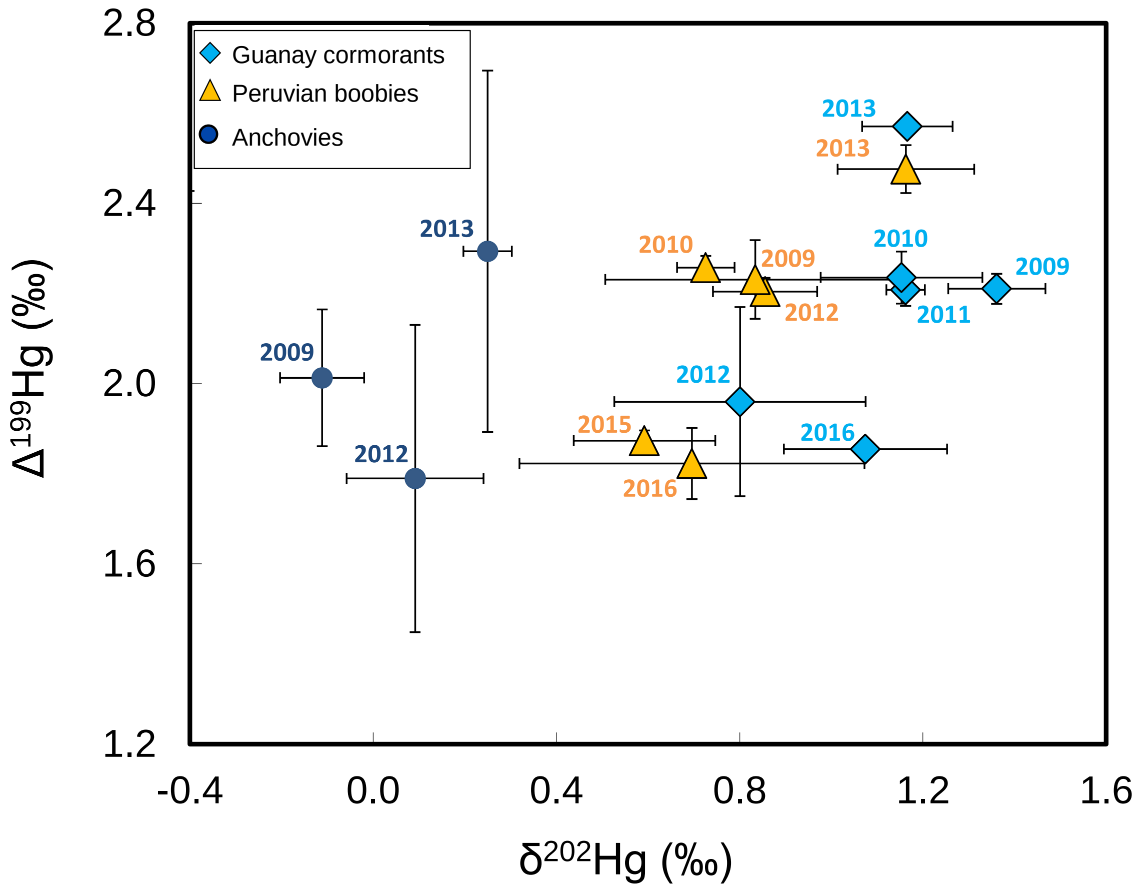

Figure 3. Annually averaged values of Hg odd-MIF *versus* Hg MDF values (Δ^{199}Hg *versus* δ^{202}Hg) of seabirds (2009-2016) and anchovies (2009, 2012, 2013). Values are means±SD. Number of individuals: n=4-10 per species per year).

3.3 Limited influence of ENSO forcing on seabird blood Hg concentrations.

Significant interannual blood Hg variability was observed for both Guanay cormorants and Peruvian boobies (Kruskal-Wallis, H=48.3 and 55.4, respectively, both p<0.0001). In 2013, cormorants exhibited significantly higher mean Hg concentrations (1.17 ± 0.15 µg $\cdot g^{-1}$) than the rest of the years. Guanay cormorants and Peruvian boobies showed statistically lower concentrations in 2011 (0.56 ± 0.19 and 0.32 ± 0.05 µg $\cdot g^{-1}$, respectively), and during 2016, Peruvian boobies exhibited their lowest concentration of 0.21 ± 0.12 µg $\cdot g^{-1}$. Mercury concentrations of anchovies (muscle) were highly variable during the period 2009-2013 (0.08 ± 0.05, 0.01-0.23 µg $\cdot g^{-1}$, n=66) but did not show significantly different Hg concentration among years (Kruskal-Wallis, H=22.65, p=0.001) (Figure S6). When applying GAMs, the optimal model to explain the variability of Hg concentration, expressed as log(Hg), was the model including anchovy biomass, blood $\delta^{15}N$ and upwelling index together as explanatory variables (Table S2). However, this model only explained for 27 to 30% of the interannual Hg concentration trends, depending on the spatial area considered. This suggests a weak impact of the changing biogeochemical parameters on the MeHg levels at the top of food web during contrasted climatic conditions occurring on the period 2009-2016.

A recent study in the Galapagos archipelago also reported low interannual variations of feather Hg concentrations in several species of booby *Sula spp.* during the period 2011-2017 [82]. This strengthens our finding, at a much larger regional scale, showing the absence of a significant change in MeHg concentrations of third-level consumers of the marine food web under strong climate forcing conditions. The relatively stable MeHg concentrations observed in seabirds during ENSO events of high amplitude contrast with tentative modelling and experimental studies which suggested higher MeHg bioaccumulation rates in fish with increasing water temperatures [9,19,20]. Schartup et al. [9] predicted that a 1°C increase of seawater temperature would lead to a 32 and 70% increase of MeHg concentrations in Atlantic cod and spiny dogfish, respectively. The same authors also suggested that dietary changes in pelagic fish in response to overfishing could lead to changes in MeHg bioaccumulation rates [9]. Contrarily, our results show that an increase of seawater temperature of 2°C during El Niño 2015-2016 (which can reach +3°C range in extreme El Niño cases [83]) did not translate into a significant impact on MeHg concentrations in top predators of the Peruvian food web, represented here by seabirds.

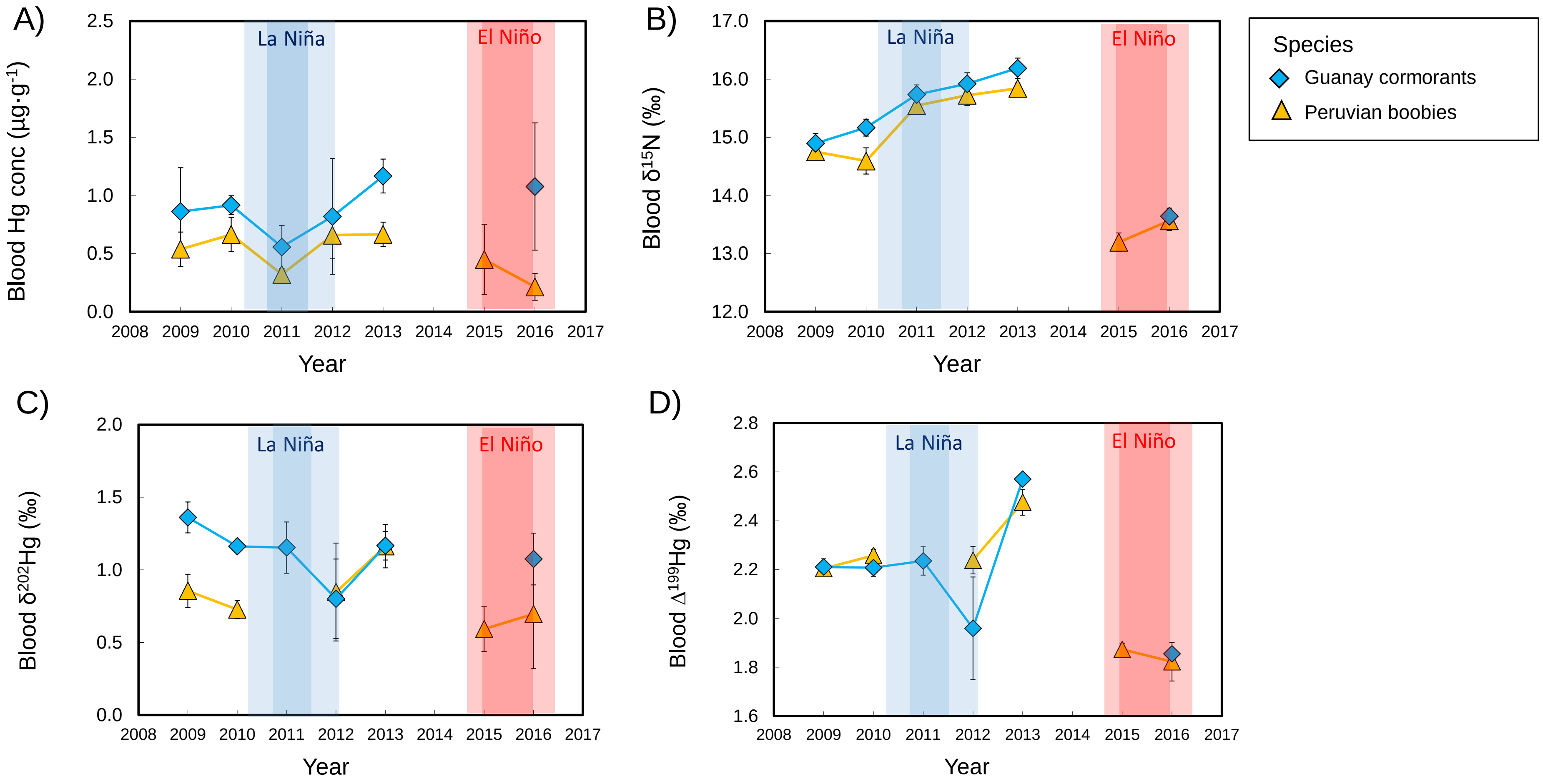

Figure 4. Interannual variations of seabird blood A) Hg concentrations (µg ·g^{-1}, dw); B) N isotopes (δ^{15}N, ‰); C) Hg MDF (δ^{202}Hg, ‰); D) Hg odd-MIF (Δ^{199}Hg, ‰). Values are Means ± SD. Number of individuals analysed: blood Hg concentration and δ^{15}N values (5-41 individuals per species per year), Hg isotope analysis (4-10 individuals, per species per year).

3.4 ENSO driven variability of nitrogen isotopes

Figure 4B shows the progressive increase of seabird $\delta^{15}N$ values from 2010 to 2013, which reached the highest mean values in 2013, both for Guanay cormorants and Peruvian boobies (16.19 ± 0.17 and 15.84 ± 0.09‰, respectively). In contrast, $\delta^{15}N$ values of seabirds decreased sharply in 2015 (boobies: 13.19 ± 0.16‰) and 2016 (cormorants: 13.64 ± 0.14‰ and boobies: 13.56 ± 0.17‰) during the El Niño event. We observed significant interannual variations of blood $\delta^{15}N$ values of cormorants and boobies (Kruskal Wallis, H=91.3 and 97.8 respectively, both $p<0.0001$). Interestingly, the observation of a limited interspecies difference in $\delta^{15}N$ (0.2 to 0.5‰) among all years, in the context of following similar and parallel interannual trends capturing the exact same $\delta^{15}N$ drop of ~2.5‰ in 2015-2016 (which corresponds in theory to a change close of one trophic level) is inconsistent with the idea that it might be caused by a change in diet for the two seabird species. The vertical movements of anchovies to deeper zones during El Niño [75] could lead to higher foraging specialisation of the two seabird species due to higher competition for prey, as documented in other booby species [84]. Therefore, we would expect that significant changes in the diet of seabirds could lead to high inter-species differences in $\delta^{15}N$ values during years of less prey abundance, but we did not observe this trend during our studied period. A pronounced baseline shift in $\delta^{15}N$ translated into the local food chain, caused by a change in nutrient regimes related to the upwelling dynamics driven by ENSO [76] is most likely the driving factor. Indeed, despite $\delta^{15}N$ represents a unique proxy to document trophic interactions and seabird diet in most ecosystems, the singularity of the upwelling regime on the N cycle operating at the baseline level of the NHCS is known to induce significant $\delta^{15}N$ baseline shifts translated up to marine predators [46,47]. This finding is consistent with (i) field observations confirming that anchovy was almost the sole species observed in seabird regurgitates for all years, (ii) that the biomass of anchovies has decreased and stayed low as soon as 2012 (Figure 2F), not influencing the $\delta^{15}N$ shift in seabirds during the same period of time, and (iii) that the interannual differences in $\delta^{13}C$ and $\delta^{15}N$ in the two seabird species reflect those in anchovies for the same years (Figure S4). Baseline processes are thus mostly responsible for the interannual differences in $\delta^{15}N$ values in seabird blood.

Marine oxygen consumption strongly determines N-loss processes, such as denitrification and anammox [85], that induce significant N isotopic fractionation. Anaerobic bacteria use nitrate (NO_3^-) as an oxidant for the degradation of organic matter and its reduction produces isotopically light products (N_2 and N_2O) and isotopically heavier residual nitrate [86,87]. Also, anaerobic ammonia (NH_4^+) oxidation (annamox) is likely the predominant pathway for N loss in oceanic OMZs [88]. Both heterotrophic denitrification and anammox processes appear to decrease significantly under El Niño conditions [89], coupled to low primary productivity, the deepening of the OMZ distribution and high bottom water oxygenation. Therefore, lower organic matter mineralization and limited nitrate supply to surface waters under El Niño conditions depletes isotopically the particulate organic matter utilized by phytoplankton, leading to lower $\delta^{15}N$ values in biota [89,90]. Consequently, the significant interannual variations of seabird $\delta^{15}N$ are more likely related to shifts in the N isotopic baseline and therefore can be used as a proxy of oxygenation events/organic matter remineralization, like El Niño or the warm ENSO events of the NHCS [91].

3.5 ENSO driven variability in Hg isotopes

Despite the absence of substantial changes in Hg concentration in biota over the studied period, we detected an enhanced interannual variability of seabird Hg isotopes (Figure 4C-D). We observed no linear relationship of $\delta^{202}Hg$ with ENSO events proxied by ICEN index ($p=0.08$) and no significant $\delta^{202}Hg$ interannual variations neither for cormorants (Kruskal Wallis, $H=17.1$, $p=0.004$) nor boobies ($H=16.4$, $p=0.006$). The GAM applied for $\delta^{202}Hg$ showed that the best explanatory variables are $\delta^{15}N$, upwelling index and NPP together, but only explained for 36 to 40% of the total $\delta^{202}Hg$ variability, depending on the integrated area (Table S2).

Interannual variability of Δ^{199}Hg of Guanay cormorants and Peruvian boobies was significant (Kruskal Wallis, H=28.8 and 32.21 respectively, both p<0.0001) and lower Δ^{199}Hg values were observed during El Niño years relative to La Niña and normal years for both species (H=24.02, p<0.0001) (Figure 4D). Both Guanay cormorants and Peruvian boobies exhibited higher Δ^{199}Hg values in 2013 (2.57 ± 0.02 and 2.48 ± 0.05‰), with a pronounced significant decrease in 2015 (boobies: 1.87 ± 0.02‰) and 2016 (cormorants: 1.85 ± 0.02 and boobies: 1.82 ± 0.08‰). Significant linear relationships were found between Δ^{199}Hg and δ^{15}N values of cormorants (R^2=0.59, p<0.001) and boobies (R^2=0.77, p<0.001), suggesting that both isotopic signatures are biogeochemically related and that interannual variations in Δ^{199}Hg and δ^{15}N values are not trophic or ecologically driven. Additionally, results of GAM showed that seabird Δ^{199}Hg are strongly explained by oxycline depth, SST and NPP, explaining for 77% of the Δ^{199}Hg internannual variability (Table S2).

Due to the sensitivity of Δ^{199}Hg to sea-surface MeHg photochemical reactions, these results suggest that seabird Δ^{199}Hg values likely reflect the change at which MeHg is formed and photodegraded, mirroring the oxycline depth oscillations during ENSO events. Indeed, the sharp decrease of seabird Δ^{199}Hg values during the El Niño 2015-2016 (down to ~1.8‰) is coincident with a deepening of the oxycline from 30-50 m to 100 m depth (Figure 2D), and therefore likely reflects a larger contribution of deeper and less photodegraded MeHg production. Oxycline depth variability has a direct impact on the biogeochemical processes of the northern region of the NHCS because oxygen is a control factor in the distribution of many organisms [53,92]. The bottom depth of the oxycline is the zone where the most intense particulate organic matter remineralization occurs, an essential process for the maintenance of the Peru OMZ [93] and Hg methylation. Vertical profiles across a large coastal-oceanic section off Peru have shown maxima of MeHg concentrations within the OMZ and near the subsurface chlorophyll maximum [25], that are expected to be driven by *in situ* microbial methylation in these coastal productive areas. During El Niño episodes, the deepening of the oxycline can favour the expansion of the vertical habitat of most marine organisms into deeper zones of the water column that are less connected to the photic zone. In contrast, the sudden increase of seabird Δ^{199}Hg values from 2012 to 2013 is coincident with an increase of δ^{15}N values, and of shallower oxycline (Figure 2D), likely favouring MeHg formation and photodegradation near the surface in 2013 in the context of a compressed habitat for anchovy schools.

Our results showing profound changes in the depth at which MeHg is formed and photodegraded while displaying a limited impact on seabird MeHg concentrations during ENSO can be explained by different factors. We consider two potential explanations for this. First, photochemical MeHg degradation may not be the dominant MeHg loss mechanism above the oxycline, leading to measurable ENSO driven Δ^{199}Hg variability but not food web MeHg variability. Second, photochemical MeHg degradation is the dominant loss mechanism, enhanced in 2013 due to the shallow oxycline. MeHg photodemethylation is balanced by enhanced inorganic Hg methylation in the OMZ due to higher primary productivity and ensuing particle remineralization and Hg methylation in the OMZ under these conditions (Figure 5). During El Niño events, the deepening of the oxycline leading to reduced MeHg photodegradation, as suggested by the drop in Δ^{199}Hg, is associated with lower vertical inputs of organic matter and remineralization traced by lower δ^{15}N, leading to lower MeHg formation. Finally, we considered the possibility that during La Niña years, a higher advection of nutrients and organic matter towards the surface increases the supply of MeHg produced at depth (with close-to zero Δ^{199}Hg values). However, this scenario would lead to a dilution of the highly photodemethylated MeHg in the surface with MeHg from deeper zones, lowering the Δ^{199}Hg values of MeHg assimilated by biota during La Niña, which is the opposite to our observations. Consequently, our results reveal that variability in Δ^{199}Hg values of the Peruvian food web are mostly driven by changes in productivity and in oxycline depth rather than water mass mixing, and that most bioavailable MeHg is produced in the oxycline.

In summary, the strong ENSO climate variability of SST, NPP and oxycline depth in the NHCS and OMZ was not accompanied by variability in marine food web top predator MeHg concentrations. These observations contrast with recent model predictions, based on Atlantic Ocean food web data, that ocean warming and overfishing have led to increases in fish MeHg levels [9].We suggest that marine MeHg dynamics, food web uptake and bioaccumulation are more resilient to climate warming than suggested by the model developed in Schartup et al. 2019 [9]. Further research investigating other oceanic regions, and exploring different marine ecosystems are needed.

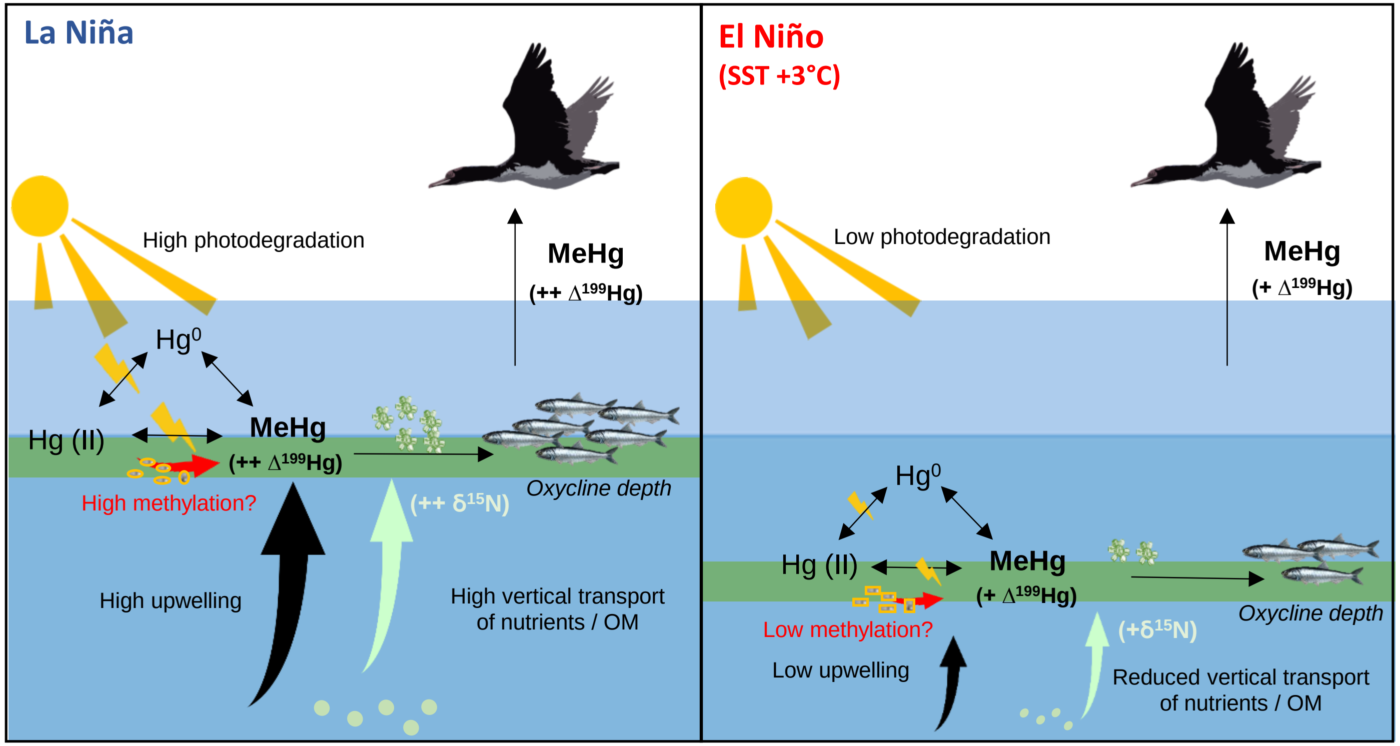

Figure 5. Schematic figure about the dominant Hg processes during contrasted ENSO events. During La Niña (left panel), the conditions of higher supply of nutrient may favour productivity potentially enhancing in situ microbial methylation/demethylation of Hg in the OMZ. However, since the oxycline is shallower, the extent of MeHg photodemethylation would be high (leading to higher Δ^{199}Hg values). Conversely, during El Niño, lower nutrient supply and remineralization may reduce microbial Hg methylation rates, and, as the oxycline is much deeper, MeHg photodegradation processes would be inhibited. Both processes (MeHg formation and MeHg degradation) seem to be compensated, leading to stable MeHg concentrations in the Peruvian food web during extreme ENSO events.

4 Acknowledgements

This work was supported by the cooperative agreement between the Institut de Recherche pour le Développement (IRD), the Peruvian Sea Institute (IMARPE), the Agence Nationale de la Recherche (ANR) project ‘Top Predators as Indicators of Exploited Marine Ecosystem dynamics’ (TOPINEME, PI SB), and the International Joint Laboratory DISCOH 1&2 for sample collection, and funding for carbon and nitrogen isotope and mercury concentration analysis. We thank Gaël Guillou for carbon and nitrogen stable isotope analysis. We thank the French National Research Agency ANR-17-CE34-0010 project ‘Unraveling the origin of methylMERcury TOXin in marine ecosystems’ (MERTOX, PI DP) for providing financial support for Hg stable isotopes analysis and for the postdoctoral grant provided to Marina Renedo.

5 Supporting information paragraph

Further experimental details of methodological approach; Statistical results of generalized additive models (GAM) models; Detailed QA/QC of Hg isotopic analyses; Complete tables of Hg concentrations and C, N and Hg isotopic results of seabirds; Supplementary figures: Figure S1, Spatial resolution of the areas integrated for satellite data; Figure S2, Results of the optimal GAM models; Figure S3, Interannual variations of 2-month averages of additional physical and biogeochemical/biological parameters in the NHCS; Figure S4, Annually averaged δ^{15}N and δ^{13}C values of blood samples of seabirds and prey; Figure S5, Δ^{199}Hg *versus* Δ^{201}Hg values of seabirds and anchovies; Figure S6, Temporal trend of Hg concentrations of anchovy samples Figure S7, Hg concentrations *versus* δ^{202}Hg values of blood samples of seabirds and anchovies.

6 References

(1) Tan, S. W.; Meiller, J. C.; Mahaffey, K. R. The Endocrine Effects of Mercury in Humans and Wildlife. *Crit. Rev. Toxicol.* **2009**, *39* (3), 228–269. https://doi.org/10.1080/10408440802233259.

(2) Li, C.; Sonke, J. E.; Le Roux, G.; Piotrowska, N.; Van Der Putten, N.; Roberts, S. J.; Daley, T.; Rice, E.; Gehrels, R.; Enrico, M.; Mauquoy, D.; Roland, T. P.; De Vleeschouwer, F. Unequal Anthropogenic Enrichment of Mercury in Earth's Northern and Southern Hemispheres. *ACS Earth Space Chem.* **2020**, *4* (11), 2073–2081. https://doi.org/10.1021/acsearthspacechem.0c00220.

(3) Outridge, P. M.; Stern, G. A.; Hamilton, P. B.; Sanei, H. Algal Scavenging of Mercury in Preindustrial Arctic Lakes. *Limnol. Oceanogr.* **2019**, *64* (4), 1558–1571. https://doi.org/10.1002/lno.11135.

(4) Kirk, J.; St. Louis, V. L.; Hintelmann, H.; Lehnherr, I.; Else, B.; Poissant, L. Methylated Mercury Species in Marine Waters of the Canadian High and Sub Arctic. *Env. Sci Technol* **2008**, *42* (22), 8367–8373. https://doi.org/10.1021/es801635m.

(5) Monperrus, M.; Tessier, E.; Amouroux, D.; Leynaert, A.; Huonnic, P.; Donard, O. F. X. Mercury Methylation, Demethylation and Reduction Rates in Coastal and Marine Surface Waters of the Mediterranean Sea. *Mar. Chem.* **2007**, *107* (1), 49–63. https://doi.org/10.1016/j.marchem.2007.01.018.

(6) Sunderland, E. M.; Krabbenhoft, D. P.; Moreau, J. W.; Strode, S. A.; Landing, W. M. Mercury Sources, Distribution, and Bioavailability in the North Pacific Ocean: Insights from Data and Models. *Glob. Biogeochem. Cycles* **2009**, *23* (2), 1–14. https://doi.org/10.1029/2008GB003425.

(7) Choy, C. A.; Popp, B. N.; Kaneko, J. J.; Drazen, J. C. The Influence of Depth on Mercury Levels in Pelagic Fishes and Their Prey. *Proc. Natl. Acad. Sci. U. S. A.* **2009**, *106* (33), 13865–13869.

(8) Streets, D. G.; Horowitz, H. M.; Lu, Z.; Levin, L.; Thackray, C. P.; Sunderland, E. M. Global and Regional Trends in Mercury Emissions and Concentrations, 2010–2015. *Atmos. Environ.* **2019**, *201* (December 2018), 417–427. https://doi.org/10.1016/j.atmosenv.2018.12.031.

(9) Schartup, A. T.; Thackray, C. P.; Qureshi, A.; Dassuncao, C.; Gillespie, K.; Hanke, A.; Sunderland, E. M. Climate Change and Overfishing Increase Neurotoxicant in Marine Predators. *Nature* **2019**, *572* (7771), 648–650. https://doi.org/10.1038/s41586-019-1468-9.

(10) Krabbenhoft, D. P.; Sunderland, E. M. Global Change and Mercury. *Science* **2013**, *341* (6153), 1457–1458. https://doi.org/10.1126/science.1242838.

(11) IPCC Working Group 1, I.; Stocker, T. F.; Qin, D.; Plattner, G.-K.; Tignor, M.; Allen, S. K.; Boschung, J.; Nauels, A.; Xia, Y.; Bex, V.; Midgley, P. M. IPCC, 2013: Climate Change 2013: The Physical Science Basis. Contribution of Working Group I to the Fifth Assessment Report of the Intergovernmental Panel on Climate Change. *Ipcc* **2013**, *AR5* (September 2014), 1535.

(12) Bindoff, N. L.; Cheung, W. W. L.; Kairo, J. G.; Aristegui, J.; Guinder, V. A.; Hallberg, R.; Hilmi, N.; Jiao, N.; Karim, M. S.; Levin, L.; O'Donoghue, S.; Purca Cuicapusa, S. R.; Rinkevich, B.; Suga, T.; Tagliabue, A.; Williamson, P. Changing Ocean, Marine Ecosystems, and Dependent Communities. *IPCC Spec. Rep. Ocean Cryosphere Chang. Clim.* **2019**, 447–588.

(13) Gregg, W. W.; Conkright, M. E.; Ginoux, P.; O'Reilly, J. E.; Casey, N. W. Ocean Primary Production and Climate: Global Decadal Changes. *Geophys. Res. Lett.* **2003**, *30* (15), 10–13. https://doi.org/10.1029/2003GL016889.

(14) Stramma, L.; Jonhson, G. C.; Sprintall, J.; Mohrholz, V. Expanding Oxygen-Minimum Zones in the Tropical Oceans. *Science* **2008**, *320*, 655–659.

(15) Diaz, R. J.; Rosenberg, R. Spreading Dead Zones and Consequences for Marine Ecosystems. *Science* **2008**, *321* (5891), 926–929. https://doi.org/10.1126/science.1156401.

(16) Cheung, W. Explaining Ocean Warming: Causes, Scale, Effects and Consequences. *Explain. Ocean Warm. Causes Scale Eff. Consequences* **2016**, No. January. https://doi.org/10.2305/iucn.ch.2016.08.en.

(17) Blanchard, J. L.; Jennings, S.; Holmes, R.; Harle, J.; Merino, G.; Allen, J. I.; Holt, J.; Dulvy, N. K.; Barange, M. Potential Consequences of Climate Change for Primary Production and Fish Production in Large Marine Ecosystems. *Philos. Trans. R. Soc. B Biol. Sci.* **2012**, *367* (1605), 2979–2989. https://doi.org/10.1098/rstb.2012.0231.

(18) Mason, R. P.; Choi, A. L.; Fitzgerald, W. F.; Hammerschmidt, C. R.; Lamborg, C. H.; Soerensen, A. L.; Sunderland, E. M. Mercury Biogeochemical Cycling in the Ocean and Policy Implications. *Environ. Res.* **2012**, *119*, 101–117. https://doi.org/10.1016/j.envres.2012.03.013.

(19) Dijkstra, J. A.; Buckman, K. L.; Ward, D.; Evans, D. W.; Dionne, M.; Chen, C. Y. Experimental and Natural Warming Elevates Mercury Concentrations in Estuarine Fish. *PLoS ONE* **2013**, *8* (3), 1–9. https://doi.org/10.1371/journal.pone.0058401.

(20) Maulvault, A. L.; Custódio, A.; Anacleto, P.; Repolho, T.; Pousão, P.; Nunes, M. L.; Diniz, M.; Rosa, R.; Marques, A. Bioaccumulation and Elimination of Mercury in Juvenile Seabass (Dicentrarchus Labrax) in a Warmer Environment. *Environ. Res.* **2016**, *149*, 77–85. https://doi.org/10.1016/j.envres.2016.04.035.

(21) Espinoza-Morriberon, D.; Echevin, V.; Colas, F.; Tam, J.; Ledesma, J.; Vasquez, L.; Graco, M. Impacts of El Niño Events on the Peruvian Upwelling System Productivity. *J. Geophys. Res. Oceans* **2017**, *122* (7), 5423–5444. https://doi.org/10.1002/2016JC012335.Received.

(22) Graco, M. I.; Purca, S.; Dewitte, B.; Castro, C. G.; Morón, O.; Ledesma, J.; Flores, G.; Gutiérrez, D. The OMZ and Nutrient Features as a Signature of Interannual and Low-Frequency Variability in the Peruvian Upwelling System. *Biogeosciences* **2017**, *14* (20), 4601–4617. https://doi.org/10.5194/bg-14-4601-2017.

(23) Chavez, F. P.; Bertrand, A.; Guevara-Carrasco, R.; Soler, P.; Csirke, J. The Northern Humboldt Current System: Brief History, Present Status and a View towards the Future. *Prog. Oceanogr.* **2008**, *79* (2–4), 95–105. https://doi.org/10.1016/j.pocean.2008.10.012.

(24) Gutiérrez, D.; Enríquez, E.; Purca, S.; Quipúzcoa, L.; Marquina, R.; Flores, G.; Graco, M. Oxygenation Episodes on the Continental Shelf of Central Peru: Remote Forcing and Benthic Ecosystem Response. *Prog. Oceanogr.* **2008**, *79* (2–4), 177–189. https://doi.org/10.1016/j.pocean.2008.10.025.

(25) Bowman, K. L.; Hammerschmidt, C. R.; Lamborg, C. H.; Swarr, G. J.; Agather, A. M. Distribution of Mercury Species across a Zonal Section of the Eastern Tropical South Pacific Ocean (U.S. GEOTRACES GP16). *Mar. Chem.* **2016**, *186,* 156–166. https://doi.org/10.1016/j.marchem.2016.09.005.

(26) Bowman, K. L.; Lamborg, C. H.; Agather, A. M. A Global Perspective on Mercury Cycling in the Ocean. *Sci. Total Environ.* **2020**, *710,* 136166. https://doi.org/10.1016/j.scitotenv.2019.136166.

(27) Apaza, M.; Figari, A. Mortandad de Aves Marinas Durante “El Niño 1997-98” En El Litoral Sur de San Juan de Marcona, ICA -Perú. *Rev. Peru. Biol.* **1999**, *6* (3), 110–117. https://doi.org/10.15381/rpb.v6i3.8436.

(28) Ñiquen, M.; Bouchon, M. Impact of El Niño Events on Pelagic Fisheries in Peruvian Waters. *Deep-Sea Res. Part II Top. Stud. Oceanogr.* **2004**, *51* (6–9), 563–574. https://doi.org/10.1016/j.dsr2.2004.03.001.

(29) Bertrand, A.; Lengaigne, M.; Takahashi, K.; Avadi, A.; Poulain, F.; Harrod, C. *El Niño Southern Oscillation (ENSO) Effects on Fisheries and Aquaculture*; 2020. https://doi.org/10.4060/ca8348en.

(30) Zavalaga, C. B.; Paredes, R. Foraging Behaviour and Diet of the Guanay Cormorant. *South Afr. J. Mar. Sci.* **1999**, No. 21, 251–258. https://doi.org/10.2989/025776199784125980.

(31) Weimerskirch, H.; Bertrand, S.; Silva, J.; Bost, C.; Peraltilla, S. Foraging in Guanay Cormorant and Peruvian Booby, the Major Guano-Producing Seabirds in the Humboldt Current System. *Mar. Ecol. Prog. Ser.* **2012**, *458*, 231–245. https://doi.org/10.3354/meps09752.

(32) Carravieri, A.; Bustamante, P.; Tartu, S.; Meillère, A.; Labadie, P.; Budzinski, H.; Peluhet, L.; Barbraud, C.; Weimerskirch, H.; Chastel, O.; Cherel, Y. Wandering Albatrosses Document Latitudinal Variations in the Transfer of Persistent Organic Pollutants and Mercury to Southern Ocean Predators. *Environ. Sci. Technol.* **2014**, *48* (24), 14746–14755. https://doi.org/10.1021/es504601m.

(33) Albert, C.; Renedo, M.; Bustamante, P.; Fort, J. Using Blood and Feathers to Investigate Large-Scale Hg Contamination in Arctic Seabirds: A Review. *Environ. Res.* **2019**, *177*. https://doi.org/10.1016/j.envres.2019.108588.

(34) Renedo, M.; Amouroux, D.; Duval, B.; Carravieri, A.; Tessier, E.; Barre, J.; Bérail, S.; Pedrero, Z.; Cherel, Y.; Bustamante, P. Seabird Tissues As Efficient Biomonitoring Tools for Hg Isotopic Investigations: Implications of Using Blood and Feathers from Chicks and Adults. *Environ. Sci. Technol.* **2018**, *52* (7), 4227–4234. https://doi.org/10.1021/acs.est.8b00422.

(35) Bearhop, S.; Ruxton, G. D.; Furness, R. W. Dynamics of Mercury in Blood and Feathers of Great Skuas. *Environ. Toxicol. Chem.* **2000**, *19* (6), 1638–1643. https://doi.org/10.1897/1551-5028(2000)019<1638:Domiba>2.3.Co;2.

(36) Renedo, M.; Amouroux, D.; Pedrero, Z.; Bustamante, P.; Cherel, Y. Identification of Sources and Bioaccumulation Pathways of MeHg in Subantarctic Penguins : A Stable Isotopic Investigation. *Sci. Rep.* **2018**, *8* (8865). https://doi.org/10.1038/s41598-018-27079-9.

(37) Renedo, M.; Bustamante, P.; Cherel, Y.; Pedrero, Z.; Tessier, E.; Amouroux, D. A “Seabird-Eye” on Mercury Stable Isotopes and Cycling in the Southern Ocean. *Sci. Total Environ.* **2020**, *742*, 140499. https://doi.org/10.1016/j.scitotenv.2020.140499.

(38) Blum, J. D.; Popp, B. N.; Drazen, J. C.; Anela Choy, C.; Johnson, M. W. Methylmercury Production below the Mixed Layer in the North Pacific Ocean. *Nat. Geosci.* **2013**, *6* (10), 879–884. https://doi.org/10.1038/ngeo1918.

(39) Li, M.; Juang, C. A.; Ewald, J. D.; Yin, R.; Mikkelsen, B.; Krabbenhoft, D. P.; Balcom, P. H.; Dassuncao, C.; Sunderland, E. M. Selenium and Stable Mercury Isotopes Provide New Insights into Mercury Toxicokinetics in Pilot Whales. *Sci. Total Environ.* **2020**, *710*, 136325. https://doi.org/10.1016/j.scitotenv.2019.136325.

(40) Bergquist, B. A.; Blum, J. D. Mass-Dependent and -Independent Fractionation of Hg Isotopes by Photoreduction in Aquatic Systems. *Science* **2007**, *318* (5849), 417–420. https://doi.org/10.1126/science.1148050.

(41) Zheng, W.; Foucher, D.; Hintelmann, H. Mercury Isotope Fractionation during Volatilization of Hg(0) from Solution into the Gas Phase. *J. Anal. At. Spectrom.* **2007**, *22* (9), 1097. https://doi.org/10.1039/b705677j.

(42) Le Croizier, G.; Lorrain, A.; Sonke, J. E.; Jaquemet, S.; Schaal, G.; Renedo, M.; Besnard, L.; Cherel, Y.; Point, D. Mercury Isotopes as Tracers of Ecology and Metabolism in Two Sympatric Shark Species. *Environ. Pollut.* **2020**, No. June, 114931. https://doi.org/10.1016/j.envpol.2020.114931.

(43) Perrot, V.; Masbou, J.; Pastukhov, M. V.; Epov, V. N.; Point, D.; Bérail, S.; Becker, P. R.; Sonke, J. E.; Amouroux, D. Natural Hg Isotopic Composition of Different Hg Compounds in Mammal Tissues as a Proxy for in Vivo Breakdown of Toxic Methylmercury. *Metallomics* **2016**, *8* (2), 170–178. https://doi.org/10.1039/C5MT00286A.

(44) Janssen, S. E.; Schaefer, J. K.; Barkay, T.; Reinfelder, J. R. Fractionation of Mercury Stable Isotopes during Microbial Methylmercury Production by Iron- and Sulfate-Reducing Bacteria. *Environ. Sci. Technol.* **2016**, *50* (15), 8077–8083. https://doi.org/10.1021/acs.est.6b00854.

(45) Kwon, S. Y.; Blum, J. D.; Carvan, M. J.; Basu, N.; Head, J. A.; Madenjian, C. P.; David, S. R. Absence of Fractionation of Mercury Isotopes during Trophic Transfer of Methylmercury to Freshwater Fish in Captivity. *Environ. Sci. Technol.* **2012**, *46* (14), 7527–7534. https://doi.org/10.1021/es300794q.

(46) Espinoza, P.; Lorrain, A.; Ménard, F.; Cherel, Y.; Tremblay-Boyer, L.; Argüelles, J.; Tafur, R.; Bertrand, S.; Tremblay, Y.; Ayón, P.; Munaron, J. M.; Richard, P.; Bertrand, A. Trophic Structure in the Northern Humboldt Current System: New Perspectives from Stable Isotope Analysis. *Mar. Biol.* **2017**, *164* (4), 0. https://doi.org/10.1007/s00227-017-3119-8.

(47) Argüelles, J.; Lorrain, A.; Cherel, Y.; Graco, M.; Tafur, R.; Alegre, A.; Espinoza, P.; Taipe, A.; Ayón, P.; Bertrand, A. Tracking Habitat and Resource Use for the Jumbo Squid Dosidicus Gigas: A Stable Isotope Analysis in the Northern Humboldt Current System. *Mar. Biol.* **2012**, *159* (9), 2105–2116. https://doi.org/10.1007/s00227-012-1998-2.

(48) Post, D. M. Using Stable Isotopes to Estimate Trophic Position: Models, Methods, and Assumptions. *Ecology* **2002**, *83* (3), 703–718. https://doi.org/10.1890/0012-9658(2002)083[0703:USITET]2.0.CO;2.

(49) Cherel, Y.; Hobson, K. A. Geographical Variation in Carbon Stable Isotope Signatures of Marine Predators : A Tool to Investigate Their Foraging Areas in the Southern Ocean. *Mar. Ecol. Prog. Ser.* **2007**, *329*, 281–287.

(50) Bertrand, S.; Díaz, E.; Lengaigne, M. Patterns in the Spatial Distribution of Peruvian Anchovy (Engraulis Ringens) Revealed by Spatially Explicit Fishing Data. *Prog. Oceanogr.* **2008**, *79* (2–4), 379–389. https://doi.org/10.1016/j.pocean.2008.10.009.

(51) Gutiérrez, M.; Swartzman, G.; Bertrand, A.; Bertrand, S. Anchovy (Engraulis Ringens) and Sardine (Sardinops Sagax) Spatial Dynamics and Aggregation Patterns in the Humboldt Current Ecosystem, Peru, from 1983-2003. *Fish. Oceanogr.* **2007**, *16* (2), 155–168. https://doi.org/10.1111/j.1365-2419.2006.00422.x.

(52) Gutiérrez, M.; Castillo, R.; Segura, M.; Peraltilla, S.; Flores, M. Trends in Spatio-Temporal Distribution of Peruvian Anchovy and Other Small Pelagic Fish Biomass from 1966-2009. *Lat. Am. J. Aquat. Res.* **2012**, *40* (3 SPL. ISS.), 633–648. https://doi.org/10.3856/vol40-issue3-fulltext-12.

(53) Bertrand, A.; Ballón, M.; Chaigneau, A. Acoustic Observation of Living Organisms Reveals the Upper Limit of the Oxygen Minimum Zone. *PLoS ONE* **2010**, *5* (4). https://doi.org/10.1371/journal.pone.0010330.

(54) Espinoza-morriberón, D.; Echevin, V.; Colas, F.; Tam, J. Oxygen Variability During ENSO in the Tropical South Eastern Pacific. **2019**, No. January. https://doi.org/10.3389/fmars.2018.00526.

(55) Simmonds, E. J.; Gutiérrez, M.; Chipollini, A.; Gerlotto, F.; Woillez, M.; Bertrand, A. Optimizing the Design of Acoustic Surveys of Peruvian Anchoveta. *ICES J. Mar. Sci.* **2009**, *66* (6), 1341–1348. https://doi.org/10.1093/icesjms/fsp118.

(56) Food and Agriculture Organization of the United Nations (FAO) www.fao.org/publications.

(57) Anuario Estadístico Pesquero y Acuícola, Ministerio de Produccion del Perú https://ogeiee.produce.gob.pe/index.php/en/oee-documentos-publicaciones/publicaciones-anuales?start=0.

(58) Takahashi, K.; Mosquera, K.; Reupo, J. El Índice Costero El Niño (ICEN): Historia y Actualización. *Bol. Téc. Gener. Model. Climáticos Para El Pronóstico Ocurr. Fenóm. El Niño* **2014**, *1*, 2–4.

(59) R Core Team, 2016: A Language and Environment for Statistical Computing. R Foundation for Statistical Computing, Vienna, Austria.

(60) Burnham, K. P.; Anderson, D. R. Multimodel Inference: Understanding AIC and BIC in Model Selection. *Sociol. Methods Res.* **2004**, *33* (2), 261–304. https://doi.org/10.1177/0049124104268644.

(61) Wood, S.; Wood, M. S. *Package "Mgcv". R Package Version (No. 1.8-28).*

(62) Zuur, A. F.; Ieno, E. N.; Walker, N. J.; Saveliev, A. A.; Smith, G. M. Mixed Effects Models and Extensions in Ecology with R. *J. Stat. Softw.* **2009**, *32* (Book Review 1), 1–4. https://doi.org/10.18637/jss.v032.b01.

(63) ENFEN. *Definición Operacional de Los Eventos El Niño y La Niña y Sus Magnitudes En La Costa Del Perú*; 2012.

(64) Dewitte, B.; Vazquez-Cuervo, J.; Goubanova, K.; Illig, S.; Takahashi, K.; Cambon, G.; Purca, S.; Correa, D.; Gutierrez, D.; Sifeddine, A.; Ortlieb, L. Change in El Niño Flavours over 1958-2008: Implications for the Long-Term Trend of the Upwelling off Peru. *Deep-Sea Res. Part II Top. Stud. Oceanogr.* **2012**, *77–80*, 143–156. https://doi.org/10.1016/j.dsr2.2012.04.011.

(65) Takahashi, K.; Montecinos, A.; Goubanova, K.; Dewitte, B. ENSO Regimes: Reinterpreting the Canonical and Modoki El Nio. *Geophys. Res. Lett.* **2011**, *38* (10), 1–5. https://doi.org/10.1029/2011GL047364.

(66) Kessler, W. S. The Circulation of the Eastern Tropical Pacific: A Review. *Prog. Oceanogr.* **2006**, *69* (2–4), 181–217. https://doi.org/10.1016/j.pocean.2006.03.009.

(67) Stramma, L.; Fischer, T.; Grundle, D. S.; Krahmann, G.; Bange, H. W.; Marandino, C. A. Observed El Niño Conditions in the Eastern Tropical Pacific in October 2015. *Ocean Sci.* **2016**, *12* (4), 861–873. https://doi.org/10.5194/os-12-861-2016.

(68) Pennington, J. T.; Mahoney, K. L.; Kuwahara, V. S.; Kolber, D. D.; Calienes, R.; Chavez, F. P. Primary Production in the Eastern Tropical Pacific: A Review. *Prog. Oceanogr.* **2006**, *69* (2–4), 285–317. https://doi.org/10.1016/j.pocean.2006.03.012.

(69) Lehodey, P.; Bertrand, A.; Hobday, A. J.; Kiyofuji, H.; McClatchie, S.; Menkès, C. E.; Pilling, G.; Polovina, J.; Tommasi, D. ENSO Impact on Marine Fisheries and Ecosystems. **2020**, No. November, 429–451. https://doi.org/10.1002/9781119548164.ch19.

(70) Barbraud, C.; Bertrand, A.; Bouchón, M.; Chaigneau, A.; Delord, K.; Demarcq, H.; Gimenez, O.; Torero, M. G.; Gutiérrez, D.; Oliveros-Ramos, R.; Passuni, G.; Tremblay, Y.; Bertrand, S. Density Dependence, Prey Accessibility and Prey Depletion by Fisheries Drive Peruvian Seabird Population Dynamics. *Ecography* **2018**, *41* (7), 1092–1102. https://doi.org/10.1111/ecog.02485.

(71) Renedo, M.; Pedrero, Z.; Amouroux, D.; Cherel, Y.; Bustamante, P. Mercury Isotopes of Key Tissues Document Mercury Metabolic Processes in Seabirds. *Chemosphere* **2021**, *263*, 127777. https://doi.org/10.1016/j.chemosphere.2020.127777.

(72) Miller, T. W.; Brodeur, R. D.; Rau, G. H. Carbon Stable Isotopes Reveal Relative Contribution of Shelf-Slope Production to the Northern California Current Pelagic Community. *Limnol. Oceanogr.* **2008**, *53* (4), 1493–1503. https://doi.org/10.4319/lo.2008.53.4.1493.

(73) Passuni, G.; Barbraud, C.; Chaigneau, A.; Demarcq, H.; Ledesma, J.; Bertrand, A.; Castillo, R.; Perea, A.; Mori, J.; Viblanc, V. A.; Torres-Maita, J.; Bertrand, S. Seasonality in Marine Ecosystems: Peruvian Seabirds, Anchovy, and Oceanographic Conditions. *Ecology* **2016**, *97* (1), 182–193. https://doi.org/10.1890/14-1134.1.

(74) Lourey, M. J.; Trull, T. W.; Tilbrook, B. Sensitivity of Δ13C of Southern Ocean Suspended and Sinking Organic Matter to Temperature, Nutrient Utilization, and Atmospheric CO2. *Deep-Sea Res. Part Oceanogr. Res. Pap.* **2004**, *51* (2), 281–305. https://doi.org/10.1016/j.dsr.2003.10.002.

(75) Bertrand, A.; Gerlotto, F.; Bertrand, S.; Gutiérrez, M.; Alza, L.; Chipollini, A.; Díaz, E.; Espinoza, P.; Ledesma, J.; Quesquén, R.; Peraltilla, S.; Chavez, F. Schooling Behaviour and Environmental Forcing in Relation to Anchoveta Distribution: An Analysis across Multiple Spatial Scales. *Prog. Oceanogr.* **2008**, *79* (2–4), 264–277. https://doi.org/10.1016/j.pocean.2008.10.018.

(76) Yang, S.; Gruber, N.; Long, M. C.; Vogt, M. ENSO-Driven Variability of Denitrification and Suboxia in the Eastern Tropical Pacific Ocean. *Glob. Biogeochem. Cycles* **2017**, *31* (10), 1470–1487. https://doi.org/10.1002/2016GB005596.

(77) Kritee, K.; Barkay, T.; Blum, J. D. Mass Dependent Stable Isotope Fractionation of Mercury during Mer Mediated Microbial Degradation of Monomethylmercury. *Geochim. Cosmochim. Acta* **2009**, *73* (5), 1285–1296. https://doi.org/10.1016/j.gca.2008.11.038.

(78) Kritee, K.; Blum, J. D.; Barkay, T. Mercury Stable Isotope Fractionation during Reduction of Hg(II) by Different Microbial Pathways. *Environ. Sci. Technol.* **2008**, *42* (24), 9171–9177. https://doi.org/10.1021/es801591k.

(79) Kwon, S. Y.; Blum, J. D.; Chirby, M. a; Chesney, E. J. Application of Mercury Isotopes for Tracing Trophic Transfer and Internal Distribution of Mercury in Marine Fish Feeding Experiments. *Environ. Toxicol. Chem. SETAC* **2013**, *32* (10), 2322–2330. https://doi.org/10.1002/etc.2313.

(80) Laffont, L.; Sonke, J. E.; Maurice, L.; Hintelmann, H.; Pouilly, M.; Sanchez Bacarreza, Y.; Perez, T.; Behra, P. Anomalous Mercury Isotopic Compositions of Fish and Human Hair in the Bolivian Amazon. *Env. Sci Technol* **2009**, *43*, 8985–8990.

(81) Kwon, S. Y.; Blum, J. D.; Chen, C. Y.; Meattey, D. E.; Mason, R. P. Mercury Isotope Study of Sources and Exposure Pathways of Methylmercury in Estuarine Food Webs in the Northeastern U.S. *Env. Sci Technol* **2014**, *48*, 10089–10097. https://doi.org/10.1021/es5020554.ome.

(82) Zarn, A. M.; Valle, C. A.; Brasso, R.; Fetzner, W. D.; Emslie, S. D. Stable Isotope and Mercury Analyses of the Galapagos Islands Seabird Community. *Mar. Ornithol.* **2020**, *48* (1), 71–80.

(83) Picaut, J.; Hackert, E.; Busalacchi, A. J.; Murtugudde, R.; Picaut J., Hackert E., B. A. J.; Murtugudde, R.; Lagerloef, G. S. E. Mechanisms of the 1997–1998 El Niño–La Niña, as Inferred from Space-Based Observations. *J. Geophys. Res.* **2002**, *107* (C5). https://doi.org/10.1029/2001jc000850.

(84) Ancona, S.; Calixto-Albarrán, I.; Drummond, H. Effect of El Niño on the Diet of a Specialist Seabird, Sula Nebouxii, in the Warm Eastern Tropical Pacific. *Mar. Ecol. Prog. Ser.* **2012**, *462* (May 2014), 261–271. https://doi.org/10.3354/meps09851.

(85) Lam, P.; Lavik, G.; Jensen, M. M.; Van Vossenberg, J. De; Schmid, M.; Woebken, D.; Gutiérrez, D.; Amann, R.; Jetten, M. S. M.; Kuypers, M. M. M. Revising the Nitrogen

Cycle in the Peruvian Oxygen Minimum Zone. *Proc. Natl. Acad. Sci. U. S. A.* **2009**, *106* (12), 4752–4757. https://doi.org/10.1073/pnas.0812444106.

(86) Granger, J.; Sigman, D. M.; Lehmann, M. F.; Tortell, P. D. Nitrogen and Oxygen Isotope Fractionation during Dissimilatory Nitrate Reduction by Denitrifying Bacteria. *Limnol. Oceanogr.* **2008**, *53* (6), 2533–2545. https://doi.org/10.4319/lo.2008.53.6.2533.

(87) Cline, J. D.; Kaplan, I. R. Isotopic Fractionation of Dissolved Nitrate during Denitrification in the Eastern Tropical North Pacific Ocean. *Mar. Chem.* **1975**, *3* (1330), 271–299.

(88) Hamersley, M. R.; Lavik, G.; Woebken, D.; Rattray, J. E.; Lam, P.; Hopmans, E. C.; Sinninghe Damsté, J. S.; Krüger, S.; Graco, M.; Gutiérrez, D.; Kuypers, M. M. M. Anaerobic Ammonium Oxidation in the Peruvian Oxygen Minimum Zone. *Limnol. Oceanogr.* **2007**, *52* (3), 923–933. https://doi.org/10.4319/lo.2007.52.3.0923.

(89) Dale, A. W.; Graco, M.; Wallmann, K. Strong and Dynamic Benthic-Pelagic Coupling and Feedbacks in a Coastal Upwelling System (Peruvian Shelf). *Front. Mar. Sci.* **2017**, *4* (FEB), 1–17. https://doi.org/10.3389/fmars.2017.00029.

(90) Kock, A.; Arevalo-Martinez, D. L.; Loscher, C. R.; Bange, H. W. Extreme N2O Accumulation in the Coastal Oxygen Minimum Zone off Peru. *Biogeosciences* **2016**, *13* (3), 827–840. https://doi.org/10.5194/bg-13-827-2016.

(91) Mollier-Vogel, E.; Ryabenko, E.; Martinez, P.; Wallace, D.; Altabet, M. A.; Schneider, R. Nitrogen Isotope Gradients off Peru and Ecuador Related to Upwelling, Productivity, Nutrient Uptake and Oxygen Deficiency. *Deep-Sea Res. Part Oceanogr. Res. Pap.* **2012**, *70*, 14–25. https://doi.org/10.1016/j.dsr.2012.06.003.

(92) Bertrand, A.; Chaigneau, A.; Peraltilla, S.; Ledesma, J.; Graco, M.; Monetti, F.; Chavez, F. P. Oxygen: A Fundamental Property Regulating Pelagic Ecosystem Structure in the Coastal Southeastern Tropical Pacific. *PLoS ONE* **2011**, *6* (12), 2–9. https://doi.org/10.1371/journal.pone.0029558.

(93) Paulmier, A.; Ruiz-Pino, D.; Garçon, V.; Farías, L. Maintaining of the Eastern South Pacific Oxygen Minimum Zone (OMZ) off Chile. *Geophys. Res. Lett.* **2006**, *33* (20), 2–7. https://doi.org/10.1029/2006GL026801.